

# **A 13   Dynamical Mean Field Theory**

A. Liebsch

Institut für Festkörperforschung

Forschungszentrum Jülich GmbH

## **Contents**

<b>1</b>	<b>Introduction</b>	<b>2</b>
<b>2</b>	<b>Dynamical Mean Field Theory</b>	<b>2</b>
<b>3</b>	<b>Mott transition in half-filled single band</b>	<b>6</b>
<b>4</b>	<b><math>\text{SrVO}_3</math> : evidence for local Coulomb correlations</b>	<b>7</b>
<b>5</b>	<b><math>\text{SrVO}_3</math>: enhanced Coulomb correlations at surfaces</b>	<b>8</b>
<b>6</b>	<b>From <math>\text{SrVO}_3</math>, <math>\text{CaVO}_3</math> to <math>\text{LaTiO}_3</math>, <math>\text{YTiO}_3</math>: Mott transition</b>	<b>9</b>
<b>7</b>	<b><math>\text{Na}_x\text{CoO}_2</math>: correlation induced change of Fermi surface</b>	<b>10</b>
<b>8</b>	<b>Summary</b>	<b>12</b>

# 1 Introduction

The electronic properties of materials involving transition metal ions are a challenging topic in theoretical condensed matter physics. Electrons in partly filled  $d$  or  $f$  shells are spatially confined to nearly atomic-like orbitals and repel each other via strong local Coulomb interactions. Whereas the Coulomb repulsion with other electrons at neighboring sites can be represented quite well in terms of an effective or mean field as, for instance, in density functional theory, this approach fails for the Coulomb interactions between electrons within the same shell.

Atomic-like localized interactions are most naturally described in real space. But since in these transition-metal compounds there is, of course, some wave function overlap between neighboring sites, some band formation does occur so that wave-like propagation of electrons through the crystal must also be taken into account. Thus, these systems are neither in the purely atomic limit, nor in the fully itinerant limit which is the more familiar situation in simple metals, many semiconductors, and noble metals. In solid state theory propagation via Bloch waves and band formation are most conveniently described in momentum space which allows one to take advantage of the periodicity of the crystal structure. Materials involving strongly localized electrons therefore require methods that provide some combination of momentum and real space formulations in order to handle itinerant and atomic-like features of the electronic structure on an equal basis.

An adequate description of the electronic properties of transition-metal oxides requires two main ingredients. One concerns the local Coulomb interaction in the  $d$  or  $f$  shells of the transition metal ions. These interactions have been the subject of a large variety of many-body studies. Over the past few decades several computational approaches have been developed that deal with electronic correlations on various levels of sophistication. The second important aspect concerns the complicated crystal structure, usually with several atoms and many more electrons per unit cell. Thus, the one-electron properties also require sophisticated and accurate computational methods. Occasionally, the partially filled bands near the Fermi level, which are the important ones for low-lying excitations, for transport properties, optical conductivity studies, etc., can be represented reasonably well in terms of a tight-binding picture involving few subbands. Nevertheless, the great variety of crystal structures and unit cells comprising different kinds of atoms gives rise to a wealth of different phenomena and needs to be taken into account in a sufficiently detailed manner. Fortunately, several excellent electronic structure methods are (almost) routinely available today.

The combination of both of these important aspects: adequate treatment of strong local Coulomb correlations and adequate description of complex one-electron and geometrical structures, in one common approach, has recently lead to a breakthrough in condensed matter theory in the area of strongly correlated materials. This approach is called Dynamical Mean Field Theory (DMFT) and is the subject of the present lecture [1–4].

# 2 Dynamical Mean Field Theory

The key idea underlying the DMFT is to simplify the full problem, with many-electron Coulomb interactions at every lattice site and one-electron hopping between sites, by an effective impurity problem of the following nature: the Coulomb interactions are retained only at one particular site and are replaced on all surrounding sites by a self-energy. This impurity problem is solved via a suitable many-body technique, the so-called ‘impurity solver’, where the one-electron

hopping between sites is the same as in the original problem and the self-energy is added to the local one-electron potential. The result of this impurity calculation can be expressed in terms of a new self-energy which is then equated with the one on the surrounding sites. This self-consistency condition can be satisfied in an iteration procedure, whereby one starts with some ‘input’ self-energy, and then uses the ‘output’ self-energy obtained from the impurity problem as ‘input’ for the next iteration step. Iterations are continued until the difference between input and output self-energies satisfies some predetermined accuracy criterion.

Similar self-consistency procedures have been used very successfully in many branches of physics. A famous example is the so-called ‘coherent potential approximation’ (CPA) in the theory of alloys: Here the full disorder problem is replaced by an impurity calculation for each constituent inserted into a fictitious host environment with a ‘coherent potential’ added to all surrounding sites. The average of the resulting effective impurity potentials is then equated with the ‘coherent potential’ which is subsequently used as input in the next step of the iterative procedure.

The DMFT and CPA approaches are in fact very similar: the main and important difference is that the CPA potential is a static one-electron potential accounting for the lack of spatial periodicity within the alloy, whereas the self-energy in the DMFT is a complex frequency-dependent (‘dynamical’) potential. Thus, it shifts low- and high-lying one-electron bands differently, it broadens them more or less, depending on their distance from the Fermi level, and it even can create new states, so-called ‘satellites’, that were not part of the original one-electron Hamiltonian.

Within the DMFT formalism the electrons at the impurity site interact not only with one another but also with a surrounding ‘bath’ which contains (i) the full complexity of the one-electron band structure and (ii) the complex self-energy that scatters and broadens the impurity levels. Converting frequencies to times this means that the DMFT accounts for the real-time dynamics of the electrons within a quasi-localized atomic shell, and for the temporary scattering processes involving neighboring sites where they experience the one-electron potential and the additional complex self-energy.

All three of these ‘self-energy’ effects: level shifts, level broadening, and extra ‘satellites’, are quite familiar from photoemission spectra. They are the natural consequence of creating a photohole in the conduction band to which the remaining electrons respond because of the Coulomb attraction.

An essential feature of the DMFT outlined above is that the many-body lattice problem is replaced by an effective, self-consistent single-site problem. The resulting self-energy is therefore also a single-site or local property, i.e., it does not depend on crystal momentum. Effectively, we made the approximation  $\Sigma(\mathbf{k}, \omega) \rightarrow \Sigma(\omega)$ , where  $\Sigma(\mathbf{k}, \omega)$  is the true self-energy for the crystal structure under consideration. In principle, it is possible to generalize the single-site DMFT to a cluster DMFT by retaining not a single site as impurity, but a cluster of atoms. Roughly speaking, the number of sites in this cluster determines the number of  $\mathbf{k}$  points (or regions) in the Brillouin Zone at which we then obtain the self-energy. This momentum variation of the self-energy can be very important for certain properties but will not be discussed further in this lecture.

An interesting trend occurs if we consider the momentum dependence of the true self-energy  $\Sigma(\mathbf{k}, \omega)$  in higher spatial dimensions, i.e., in an artificial lattice with an increasing number of nearest neighbor atoms. It can be shown rigorously that the environment of any given atom then becomes more and more isotropic, and that, in the limit of infinite dimension, the momentum variation of  $\Sigma(\mathbf{k}, \omega)$  becomes negligibly small [5]. In other words, the self-energy depends

exclusively on single-site interactions: it becomes a truly ‘local’ property, so that  $\Sigma(\omega)$  would be exact. Of course, in real 3-dimensional structures, in particular, in transition metal oxides with important layer- or even chain-like geometric elements (i.e., with few nearest neighbors), one does not really know how large the corrections might be with respect to the limit of infinite dimensions. So in each case one should be aware of a potentially important momentum variation of  $\Sigma(\mathbf{k}, \omega)$ .

As discussed above, the DMFT involves two main ingredients: the single-particle Hamiltonian  $H(\mathbf{k})$  accounting for all band structure effects in the unit cell of the crystal structure, and the single-site many-body impurity Hamiltonian. Let us consider a transition metal oxide, such as the perovskite  $\text{SrVO}_3$ , where the important  $d$  bands near the Fermi level are of the type  $t_{2g}$  ( $d_{xy}, d_{xz}, d_{yz}$ ). All other bands, such as O  $2p$ , Sr  $5s$  and V  $e_g$  ( $d_{x^2-y^2}, d_{z^2}$ ), are filled or empty and can be neglected as long as we focus on the low-frequency excitations close to  $E_F$ . The Hamiltonian  $H(\mathbf{k})$  is in this case a (3x3) matrix which can be obtained from a tight-binding fit to the  $t_{2g}$  bands of a full band structure calculation, or via a ‘down-folding’ procedure in a LMTO calculation.

The impurity Hamiltonian involves as main input quantity the local Coulomb interaction in the orbital basis under consideration. In the case of a  $t_{2g}$  shell there are only two independent parameters given by intra- and inter-orbital Coulomb matrix elements  $U = \langle ii|ii \rangle$  and  $U' = \langle ij|ij \rangle$  ( $i \neq j$ ). Exchange interactions accounting for Hund’s rule coupling are given by  $J = \langle ij|ji \rangle = \langle ii|jj \rangle$  and are, for symmetry reasons, related to  $U$  and  $U'$  via  $U' = U - 2J$ . In principle, these Coulomb matrix elements can be calculated, but in practice they are often varied on purpose in order to investigate the characteristics of a system as a function of the ‘competition’ between  $H(\mathbf{k})$  and  $U$ .

To solve the problem of the impurity in the presence of the surrounding bath within the DMFT one makes use of a so-called ‘impurity solver’. Several methods are available which differ in numerical accuracy and computational demands: the quantum Monte Carlo (QMC) method, exact diagonalization (ED), numerical renormalization group (NRG) approach, non-crossing approximation (NCA), iterated perturbation theory (IPT). These impurity solvers focus on slightly different physical aspects of the full many-body problem at the impurity site; some are primarily useful for single- or two-band problems, others can deal with multi-band systems, or are applicable at zero and/or finite temperatures.

The main quantity of interest that can be used to analyze excitation spectra observed in photoemission measurements is the one-particle Green’s function

$$G(\mathbf{k}, \omega) = \frac{1}{\omega + \mu - H(\mathbf{k}) - \Sigma(\omega)}, \quad (1)$$

where  $\mu$  is the chemical potential and all other quantities are assumed to be matrices in orbital space. The total density of states (seen in photoemission if we ignore matrix element effects, the mean-free-path of the photoelectron, etc.) is then given by:

$$A(\omega) = -\frac{1}{\pi} \text{Im} \sum_{i,\mathbf{k}} \left( \frac{1}{\omega + \mu - H(\mathbf{k}) - \Sigma(\omega)} \right)_{ii}. \quad (2)$$

Going over to a real-space representation via  $G_{\mathbf{R},\mathbf{R}'}(\omega) = \sum_{\mathbf{k}} e^{i\mathbf{k} \cdot (\mathbf{R} - \mathbf{R}')} G(\mathbf{k}, \omega)$ , where  $\mathbf{R}, \mathbf{R}'$  denote lattice sites, the ‘local’ Green’s function  $G(\omega) = G_{\mathbf{R},\mathbf{R}}(\omega)$  is

$$G(\omega) = \sum_{\mathbf{k}} \frac{1}{\omega + \mu - H(\mathbf{k}) - \Sigma(\omega)}. \quad (3)$$

This function is now used to remove the local self-energy from the site at the origin:

$$\begin{aligned} G_0(\omega) &= G(\omega) - G(\omega)\Sigma(\omega)G_0(\omega) \\ &= [G(\omega)^{-1} + \Sigma(\omega)]^{-1}. \end{aligned} \quad (4)$$

The physical meaning of this Green's function is very important: it describes the path of an electron leaving from and returning to the central site and thereby encountering (i) via the Hamiltonian  $H(\mathbf{k})$  and the Brillouin Zone integration all the complicated one-electron aspects of the crystal structure under consideration; (ii) via the (so far unspecified) self-energy  $\Sigma(\omega)$  all the dynamical interactions caused by intra-atomic many-electron processes on neighboring sites. [Note that  $G_0(\omega)$  is *not* the independent-particle Green's function which would be obtained from Eq.(3) by omitting  $\Sigma(\omega)$ .]

The next step in the procedure is the solution of the impurity problem for a given partially occupied group of orbitals, immersed in the environment described via  $G_0(\omega)$ . This problem is at the core of the DMFT and is solved by employing one of the 'impurity solvers' mentioned above. It is usually the most time-consuming part of the calculation. Apart from  $G_0(\omega)$ , the key input quantity for this step is the Coulomb interaction in the orbital basis under consideration. As mentioned above, in the case of a  $t_{2g}$  shell there are only two independent parameters given by  $U$  and  $U' = U - 2J$ .

The output of the impurity calculation is a new local Green's function  $G(\omega)$ , which in general is not the same as the  $G(\omega)$  used in the construction of  $G_0(\omega)$ . Applying the self-consistency condition, we may use this output  $G(\omega)$ , however, to find a new self-energy (see Eq. (4)):

$$\Sigma(\omega) = G_0(\omega)^{-1} - G(\omega)^{-1}. \quad (5)$$

In practice, one can start the iteration procedure with  $\Sigma(\omega) = 0$ , i.e., with  $G_0(\omega) = G(\omega)$ . Convergence is often achieved after 10 to 20 iterations; close to phase transitions many more iterations can be required. Schematically therefore a DMFT calculation proceeds via the following steps (assuming  $H(\mathbf{k})$  is available):

1. construct start self-energy  $\Sigma(\omega)$ , e.g.,  $\Sigma(\omega) = 0$
2. calculate  $G(\omega)$  via Eq.(3)
3. calculate  $G_0(\omega)$  via Eq.(4)
4. calculate new  $G(\omega)$  from  $G_0(\omega)$  via impurity solver
5. calculate new  $\Sigma(\omega)$  via Eq.(5)
6. return to step 2. by inserting new  $\Sigma(\omega)$  into Eq.(3), etc.

So far we have assumed zero temperature. For many phenomena it is important to study the behavior of system properties at finite  $T$ , for instance, the metal insulator transition that may take place as the temperature is modified. DMFT calculations are then conveniently performed in *imaginary* time/frequency space. Thus, instead of Eq.(3) we use [2]

$$\begin{aligned} G(i\omega_n) &= \sum_{\mathbf{k}} \frac{1}{i\omega_n + \mu - H(\mathbf{k}) - \Sigma(i\omega_n)} = \int_0^\beta d\tau e^{i\omega_n \tau} G(\tau) \\ G(\tau) &= \sum_n e^{-i\omega_n \tau} G(i\omega_n), \end{aligned} \quad (6)$$

where  $\omega_n = (2n + 1)\pi/\beta$  are Matsubara frequencies ( $n \geq 0$ ) and  $\beta = 1/k_B T$ . All equations given above for real  $\omega$  hold equally at imaginary  $i\omega_n$ .

### 3 Mott transition in half-filled single band

Although some of the impurity solvers are computationally very complex, there are simple approximate ones that nevertheless capture very interesting and important features, such as the Mott transition in a half-filled single band. One of these methods is the so-called iterated perturbation theory (IPT) in which the self-energy is approximated by the second-order term in a perturbation expansion [2]:

$$\Sigma(i\omega_n) = U^2 \int_0^\beta d\tau e^{i\omega_n \tau} G_0^3(\tau). \quad (7)$$

Assuming a Bethe lattice with a semi-circular density of states  $\rho(\omega) = (2/\pi)\sqrt{1-\omega^2}$  (width  $W = 2$ ),  $G(i\omega_n)$  is given by

$$G(i\omega_n) = \int d\omega \frac{\rho(\omega)}{i\omega_n + \mu - \omega - \Sigma(i\omega_n)} = 2z(1 - \sqrt{1-z^{-2}}) \quad (8)$$

where  $\mu = 0$  for half-filling and  $z = i\omega_n - \Sigma(i\omega_n)$ . The first-order Hartree-Fock self-energy  $U/2$  has been combined with  $\mu$ . At  $T = 0$  the imaginary part of the self-energy is given by

$$\text{Im } \Sigma(\omega) = U^2 \left( \int_0^\infty \int_{-\infty}^0 \int_{-\infty}^0 + \int_{-\infty}^0 \int_0^\infty \int_0^\infty \right) d\omega_{1,2,3} \rho(\omega_1) \rho(\omega_2) \rho(\omega_3) \delta(\omega + \omega_1 - \omega_2 - \omega_3). \quad (9)$$

The real part can be obtained via the Kramers Kronig relation.

The result of such a DMFT calculation at  $T = 0$  is shown in Fig. 1 [6]. It illustrates several of the key features captured within the DMFT: for small  $U$ , the quasi-particle distribution is nicely metallic, with only a little band-narrowing and level-broadening due to creation of electron hole pairs. For  $U = W = 2$ , the quasi-particle peak near  $E_F = 0$  is considerably narrowed, implying a significantly enhanced effective mass, and two new features appear near both edges of the bare density of states. These ‘satellites’ are also called Hubbard bands and represent the first hint of atomic like excitations. For  $U = 3$  the ‘coherent’ quasi-particle peak is nearly a delta function,

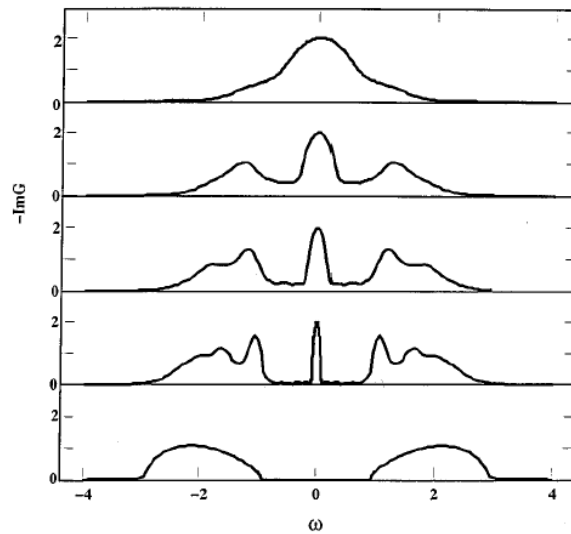


**Fig. 1:** Quasiparticle spectra for half-filled band; from top:  $U = 1, 2, 2.5, 3, 4$ ;  $W = 2$ . [6]

the system is barely metallic, and almost all of the spectral weight is located in the ‘incoherent’ satellites. Finally, for  $U = 4$  the metallic density of states near  $E_F$  has vanished and we have an insulator with two peaks located approximately at  $\pm U/2$ .

This picture conveys the metal-insulator or Mott transition, resulting from a competition of local Coulomb interactions and kinetic energy represented by the band width  $W$ . For the present IPT impurity solver, the transition occurs at  $U_c = 3.4$ . More sophisticated methods yield  $U_c = 2.9$ , but provide a qualitatively similar picture for the gradual transfer of spectral weight from the low-frequency region near  $E_F$  to the Hubbard bands as  $U$  is increased. It is this redistribution of spectral weight caused by local correlations that is impossible to describe within the LDA or purely static mean field extensions such as the LDA+U [7]. As will be seen in the examples discussed below, many transition metal oxides fall in the region  $W \approx U$ , where the quasi-particle spectra exhibit clear signs of itinerant as well as atomic-like behavior.

## 4 $\text{SrVO}_3$ : evidence for local Coulomb correlations

$\text{SrVO}_3$  can be considered as a prototype of a cubic perovskite material. V and Sr atoms form two interpenetrating simple cubic lattices, with O atoms halfway between V atoms forming cornersharing octahedra. The one-electron structure is rather simple, with one  $d$  electron per transition metal ion. LDA electronic structure calculations show that the conduction bands near the Fermi level consist of three degenerate  $t_{2g}$  bands derived from  $\text{V}^{4+}$  ions. The filled O 2p bands are separated from the  $t_{2g}$  levels by a gap of about 1 eV, and the cubic crystal field of the V-O octahedra shifts the V  $e_g$  bands above the  $t_{2g}$  bands. Because of the cubic symmetry, the  $t_{2g}$  bands can be represented quite accurately via a simple tight-binding  $3 \times 3$  Hamiltonian with only diagonal elements. Because of the cubic crystal structure, all three  $t_{2g}$  orbitals have identical density of states.

Fig. 2 shows the bandstructure of  $\text{SrVO}_3$  and the bulk density of states. Because of the dominant intra-planar hopping, there is a van Hove singularity at 1 eV above  $E_F$  due to the flat bands near M in the Brillouin Zone. This peak is not at the center of the spectrum because of important  $2^{\text{nd}}$  neighbor interactions. (The surface density of states will be discussed in the next Section.) The width of the  $t_{2g}$  bands is only about 2.5 eV, much smaller than the on-site Coulomb interaction between  $d$  electrons, which is estimated to be about 5 eV. It is to be expected, therefore, that correlations should lead to a significant redistribution of spectral weight.

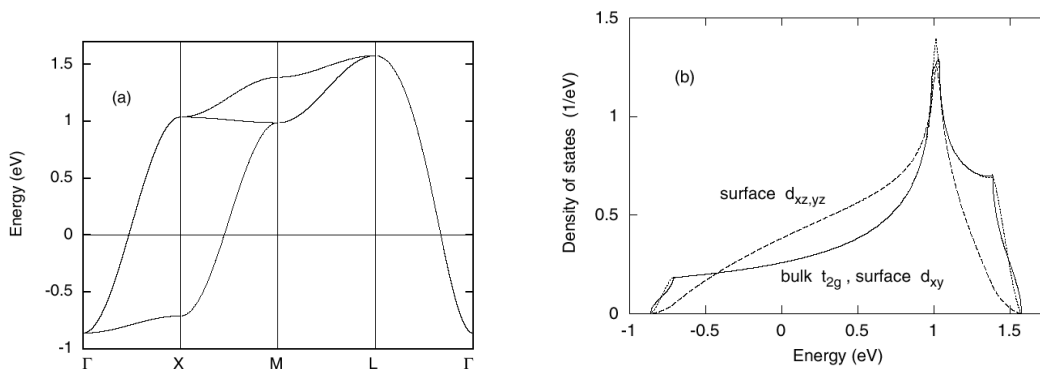


**Fig. 2:** (a) Tight-binding fit to  $t_{2g}$  bulk bands of  $\text{SrVO}_3$  ( $E_F = 0$ ). (b) Solid curve: bulk density of states; dashed and dotted curves: surface local density of  $xz, yz$  and  $xy$  states [8].

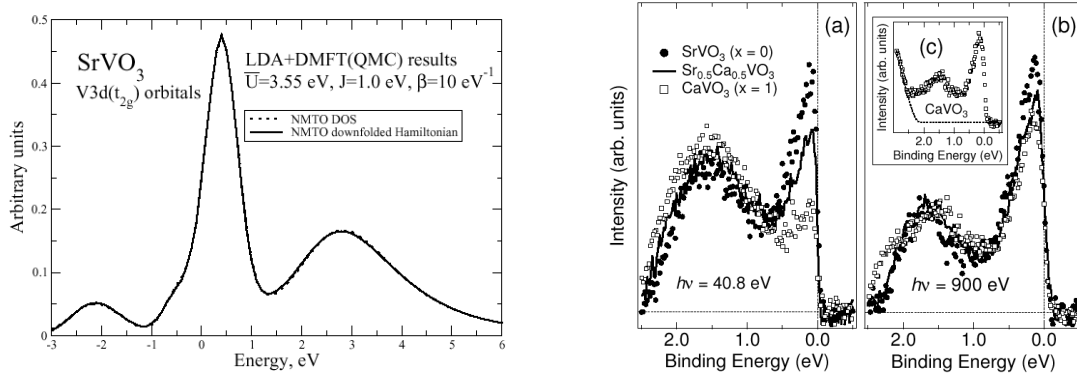


**Fig. 3:** Left: Quasi-particle spectrum of  $\text{SrVO}_3$  calculated within QMC/DMFT for  $U = 5.55$  eV,  $T \approx 10^3$  K [9]. Right: Photoemission spectra at low and high photon energies [10].

A treatment of local correlations within the DMFT, using the Quantum Monte Carlo technique to solve for the single site many body impurity problem, shows indeed that the quasi-particle spectrum of  $\text{SrVO}_3$  differs greatly from the bare bulk density of states shown in Fig. 2(b) [9]. As can be seen in Fig. 3(a), the spectral weight in the band region is shifted appreciably towards  $E_F$  (the van Hove peak in the DOS at 1 eV now lies at 0.5 eV) and a large fraction of the spectral weight has been transferred to the regions below and above the one-electron bands, in analogy to the single-band case shown in Fig. 1. These satellites are the Hubbard bands discussed above and reflect the partly atomic nature of the V  $3d t_{2g}$  excitation spectrum. This kind of shifting and broadening of states is very characteristic of correlation-induced many-electron effects. The calculated trends found for the occupied part of the spectrum agree qualitatively with the photoemission spectra shown in Fig. 3(b). The unoccupied region of the quasi-particle distribution can be compared with inverse photoemission spectra. Note that the famous 6 eV satellite observed in photoemission spectra below the  $d$  band of Ni has the same physical origin as the Hubbard peaks seen in Fig. 3.

## 5 $\text{SrVO}_3$ : enhanced Coulomb correlations at surfaces

The photoemission spectra shown in Fig. 3 indicate a striking variation with photonenergy. Similar trends are observed for many systems and are related to the surface sensitivity of this experiment: at low photon energies the mean-free-path of the emitted electron is rather short, i.e., the spectra provide more information on correlations near the surface.

A careful identification of surface effects in photoemission spectra of strongly correlated materials is important in order not to misinterpret certain correlation features as bulk-induced. For example, on the basis of earlier photoemission data, Coulomb correlations in  $\text{SrVO}_3$  and  $\text{CaVO}_3$  were at first believed to be much stronger than bulk probes such as conductivity or specific heat measurements seemed to indicate. Similarly, the Fermi surface of  $\text{Sr}_2\text{RuO}_4$  initially observed in photoemission was in striking conflict with de Haas van Alphen data for the bulk material. After several years of intense controversies involving many research groups, with many Physical Review Letters advocating one or the other viewpoint, both problems were finally resolved by identifying and separating surface features. Happily, the remaining ‘true’ bulk spectra were then found to be well consistent with other bulk-sensitive measurements.



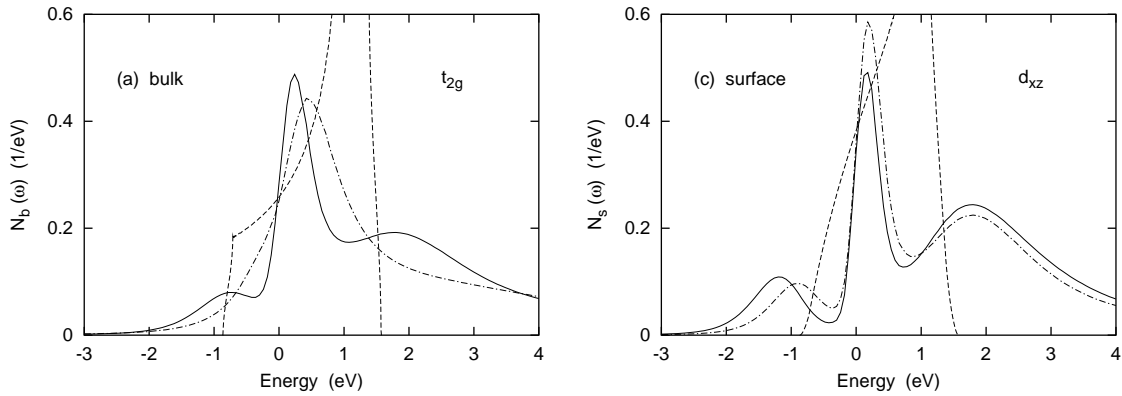


**Fig. 4:** Quasi-particle spectra of  $\text{SrVO}_3$  calculated within the QMC/DMFT for  $U = 4.3$  eV (solid curves) and  $U = 4.0$  eV (dot-dashed curves): (a) bulk spectra; (b) surface spectra. Dashed curves: bulk and surface density of states as in Fig. 2(b) [8].

Why can Coulomb correlations be stronger at surfaces than in the bulk? Roughly speaking, a surface atom can be viewed as somewhere between an atom in the gas phase and a bulk atom. Screening effects in transition metals, which in the bulk dramatically reduce free-atom Coulomb energies from 10–20 eV down to 1–5 eV, should be a little less efficient at the surface. Thus, the effective value of  $U$  is presumably larger than in the bulk. One-electron effects might also contribute to the enhancement of Coulomb correlations at surfaces. For instance, because of the reduced atomic coordination there is less single-particle hopping of electrons to neighboring sites, giving rise to an effective narrowing of the ‘local band width’ in the surface layer: the well-known ‘surface band narrowing’ effect.

This effect can be seen in Fig. 2(b): Although the total band width is the same as in the bulk, the shape of the local density of states of an atom in the surface layer is much narrower than in the bulk. The resulting enhancement of correlations is illustrated in Fig. 4: Whereas in the bulk the lower Hubbard peak just begins to be seen for  $U = 4.0 \dots 4.3$  eV, at the surface the same  $U$  values produce a much larger satellite. This trend would be even more pronounced, if  $U$  would be assumed to be larger at the surface. These results explain at least in part the experimentally observed trend with photonenergy shown in Fig. 3(b).

Other surface effects, such as surface relaxation (enhanced or reduced layer spacing) or lateral reconstruction (larger surface unit cells), modified valency, or, in complex compounds such as transition metal oxides, modified stoichiometries, etc., can contribute to new electronic properties that do not occur in the bulk. This field is evidently very complex and material-specific and has not yet been extensively investigated.

## 6 From $\text{SrVO}_3$ , $\text{CaVO}_3$ to $\text{LaTiO}_3$ , $\text{YTiO}_3$ : Mott transition

As pointed out above, the electronic structure of  $\text{SrVO}_3$  is rather simple because of the perfect cubic symmetry of this material. Interestingly, if Sr is replaced iso-electronically by Ca, the slightly smaller size of Ca ions leads to octahedral distortions which lift the  $t_{2g}$  orbital degeneracy. These distortions increase considerably if we go further to  $\text{LaTiO}_3$  and  $\text{YTiO}_3$ . All of these systems have the same nominal  $3d^1$  occupancy of  $t_{2g}$  bands, but with progressively varying hybridization between these  $3d$  orbitals and neighboring O  $2p$  shells [11]. The lifting of the orbital degeneracy leads to increasing non-diagonal contributions in the density of states.

QMC/DMFT calculations for these  $3d^1$  perovskites show that the reduced degeneracy among  $t_{2g}$  orbitals and the increasing non-diagonal density of states components cause an effective reduction of one-electron hopping and an enhancement of local correlations. In the case of  $\text{LaTiO}_3$  and  $\text{YTiO}_3$  this enhancement is sufficiently strong to lead to a Mott transition. These effects will be discussed in more detail in the lecture by E. Pavarini.

These results demonstrate the extreme sensitivity of the electronic properties of transition metal compounds to small changes of key parameters. The balance between local Coulomb energy and kinetic energy associated with the band character of these materials can be rather subtle and can easily change in one or the other way, for instance, if temperature, doping concentration, external pressure, etc. are varied. Although this sensitivity is a great challenge to theoretical approaches, it is also the source of potential technological applications.

## 7 $\text{Na}_x\text{CoO}_2$ : correlation induced change of Fermi surface

In this section we discuss the effect of Coulomb correlations on the occupation of subbands that are non-degenerate as a result of the crystal structure. Whereas in a cubic environment, the three  $t_{2g}$  bands of a perovskite such as  $\text{SrVO}_3$  are degenerate (identical subband occupations in both the single- and many-electron pictures), this degeneracy is lifted in layer materials such as  $\text{Ca}_x\text{Sr}_{2-x}\text{RuO}_4$  and  $\text{Na}_x\text{CoO}_2$ . The total number of conduction electrons is, of course, the same in single- and many-electron theories. This does not necessarily hold for the subband occupations. Thus, local Coulomb correlations may transfer charge between conduction bands and thereby modify the shape of the Fermi surface.

$\text{Ca}_x\text{Sr}_{2-x}\text{RuO}_4$  and  $\text{Na}_x\text{CoO}_2$  have been studied very extensively during the recent years since they exhibit a variety of fascinating properties. Both become superconducting and both undergo Mott transitions at certain doping concentrations. The similarity - or difference - between the mechanisms responsible for the superconductivity in these oxides and in the high- $T_c$  cuprates is of great current interest.

The valence bands of the intercalated layer compound  $\text{Na}_x\text{CoO}_2$  consist of Co-derived  $t_{2g}$  states with occupancy  $3d^{5+x}$ . For  $x \approx 0.50 - 0.75$  an unusually large thermopower is observed. For  $x \approx 0.3$  hydration gives rise to a superconducting transition at 4.5 K. In a narrow region near  $x = 0.5$  the material undergoes a metal insulator transition. The end-member at  $x = 0$  with a single hole per Co atom is believed to be a Mott insulator. For  $x = 1$  the filled  $t_{2g}$  bands are

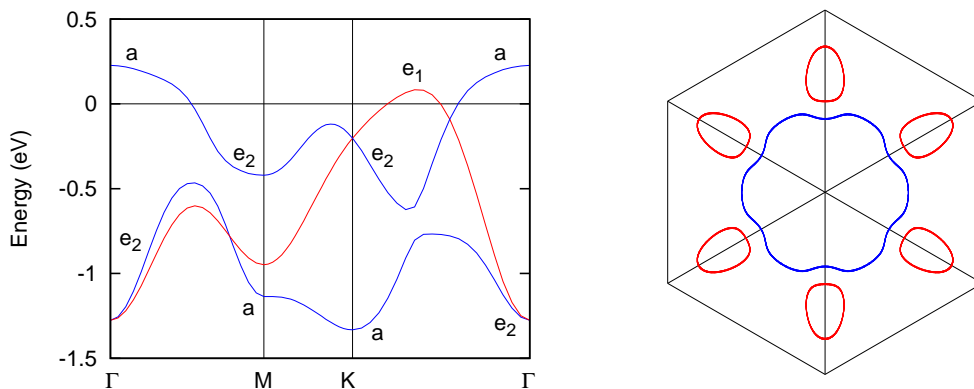


**Fig. 5:** Left: tight-binding fit to LDA bands of  $\text{Na}_{0.3}\text{CoO}_2$ ;  $E_F = 0$ ; right: Fermi surface. The  $e_{g'}$  states above  $E_F$  give rise to the small hole pockets of the Fermi surface [12].

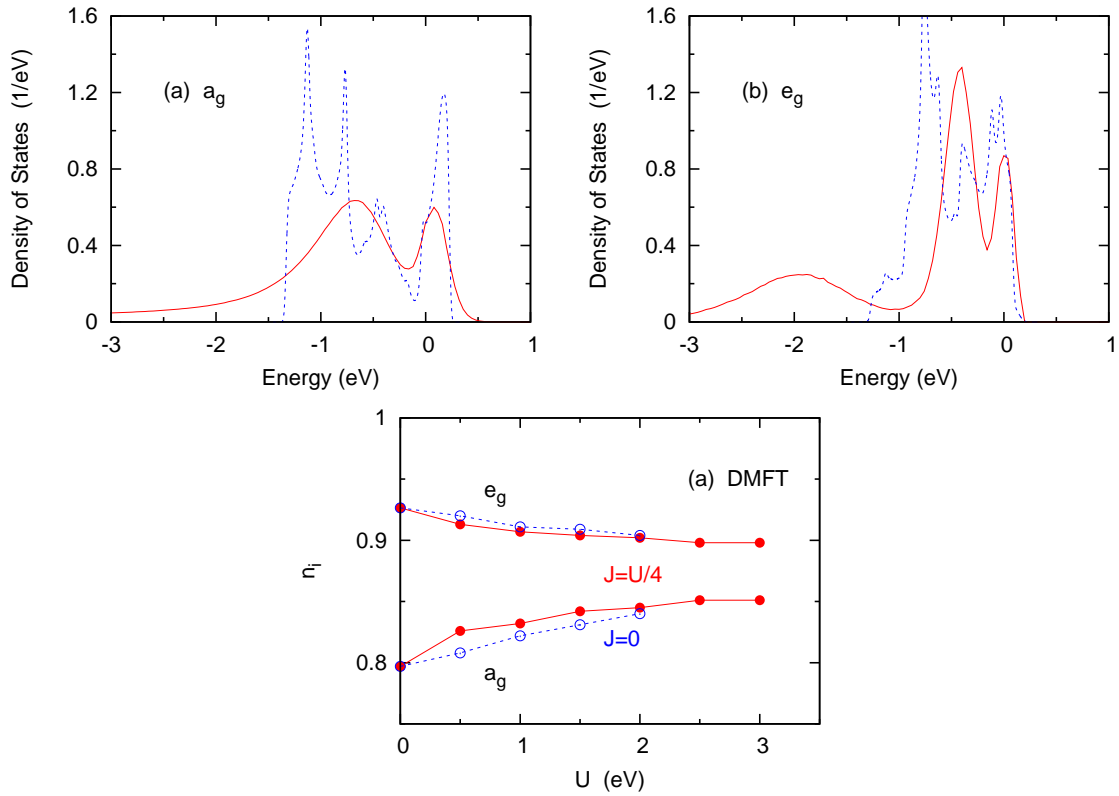


**Fig. 6:** Top: Quasi-particle spectra of  $\text{Na}_{0.3}\text{CoO}_2$  calculated within QMC/DMFT; dashed lines: density of states. Bottom: Occupations of  $a_{1g}$  and  $e_{g'}$  subbands as a function of  $U$ . Solid dots:  $J = U/4$ ; empty dots:  $J = 0$  [12].

separated by about 1.5 eV from the empty  $e_g$  bands, i.e., one has a band insulator.

Despite considerable experimental and theoretical effort, fundamental electronic properties of  $\text{Na}_x\text{CoO}_2$  such as the shape of the Fermi surface remain controversial. As shown in Fig. 5, in the metallic phase the hexagonal Fermi surface predicted by LDA band theory consists of a large hole pocket centered at  $\Gamma$  and six small hole pockets along  $\Gamma K$ . Because of the layered structure the  $t_{2g}$  levels split into an  $a_{1g}$  level and doubly degenerate  $e_{g'}$  levels, where  $a_{1g} = (d_{xy} + d_{xz} + d_{yz})/\sqrt{3}$ ,  $e_{g1} = (d_{xz} - d_{yz})/\sqrt{2}$ ,  $e_{g2} = (2d_{xy} - d_{xz} - d_{yz})/\sqrt{6}$ . The large Fermi surface stems mainly from the  $a_{1g}$  bands while the small hole pockets have predominantly  $e_{g'}$  character. The existence of these hole pockets is thought to be crucial for the understanding of the superconducting phase. On the other hand, angle resolved photoemission spectra (ARPES) provide evidence only for  $a_{1g}$  bands crossing the Fermi level. These data suggest that the  $e_{g'}$  bands are filled due to inter-orbital charge transfer not described within the LDA.

Here we discuss the possibility of modifying the Fermi surface of  $\text{Na}_{0.3}\text{CoO}_2$  via dynamical Coulomb correlations. In a single-band picture, the key effect of dynamical fluctuations is the spectral weight transfer from the quasiparticle peak near  $E_F$  to the satellites associated with the lower and upper Hubbard bands. In a multiband material, this spectral weight transfer can be orbital dependent, opening the possibility of redistributing electronic charge among the valence orbitals and modifying the shape of the Fermi surface.

Fig. 6 shows the  $a_{1g}$  and  $e_{g'}$  quasiparticle spectra for  $\text{Na}_{0.3}\text{CoO}_2$  as calculated within the DMFT. These spectra show the characteristic band narrowing near  $E_F$  caused by dynamical correlations and the transfer of weight from the coherent to the incoherent spectral region. In the narrower

$e_{g'}$  band correlations give rise to a lower Hubbard band. Also noticeable is the substantial lifetime broadening of valence states due to creation of electron hole pairs.

The occupations of these distributions are also shown in Fig. 6. For  $J = U/4$  as well as  $J = 0$ , charge transfer proceeds from  $e_{g'}$  to  $a_{1g}$ , i.e., orbital polarization is reduced. Thus, the DMFT predicts less  $e_{g'}$  occupation than the LDA, implying slightly larger  $e_{g'}$  hole pockets, in contrast to the photoemission data!

So far, there is no explanation for this striking discrepancy between the DMFT results and the ARPES measurements. On the theoretical side, the neglect of the momentum dependence of the self-energy and the approximate treatment of Hund's rule coupling (neglect of spin flip and pair-exchange terms) in the QMC method could play a role. On the experimental side, the state of the surface and possible matrix element effects have not yet been explored in detail.

## 8 Summary

The electronic properties of strongly correlated materials require a detailed description of (i) complex many-body Coulomb interactions within partially filled  $d$  or  $f$  shells, and (ii) complex one-electron features resulting from lattice geometries containing several atoms per unit cell. The Dynamical Mean Field Theory treats both aspects on the same footing. Important results of this treatment are the correlation-induced narrowing of quasi-particle peaks near  $E_F$ , the level broadening accounting for the finite lifetime of states, and the transfer of spectral weight between low and high frequencies, with the possibility of creating new states (Hubbard bands), which have no counterpart in one-electron theories.

## References

- [1] G. Kotliar and D. Vollhardt, *Physics Today*, March 2004, p.53.
- [2] For a review, see: A. Georges, G. Kotliar, W. Krauth and M. J. Rozenberg, *Rev. Mod. Phys.* **68**, 13 (1996).
- [3] A. I. Lichtenstein and M. I. Katsnelson, *Phys. Rev. B* **62**, 6884 (1998).
- [4] For a review of recent work, see: K. Held, habilitation, cond-mat/0511293.
- [5] W. Metzner and D. Vollhardt, *Phys. Rev. Lett.* **62**, 324 (1996).
- [6] X. Y. Zhang, M. J. Rozenberg, and G. Kotliar, *Phys. Rev. Lett.* **70**, 1666 (1993).
- [7] V. I. Anisimov, J. Zaanen, and O. K. Andersen, *Phys. Rev. B* **44**, 043 (1991).
- [8] A. Liebsch, *Phys. Rev. Lett.* **90**, 096401 (2003).
- [9] I. A. Nekrasov *et al.*, cond-mat/0508313.
- [10] A. Sekiyama *et al.*, *Phys. Rev. Lett.* **93**, 156402 (2004). See also: K. Maiti *et al.*, *Eurphys. Lett.* **58**, 246 (2001).
- [11] E. Pavarini *et al.*, *Phys. Rev. Lett.* **92**, 176403 (2004).
- [12] H. Ishida, M. Johannes, and A. Liebsch, *Phys. Rev. Lett.* **94**, 196401 (2005).